Chinese Journal of Oceanology and Limnology
Vol. 30 No. 6, P. 944-952, 2012
http://dx.doi.org/10.1007/s00343-012-1260-2

A dipole wind curl pattern induced by Taiwan Island and its effect on upper stratification in the northeastern South China Sea*

DENG Yi (邓奕)[1], SHI Ping (施平)[1], ZHOU Wen (周文)[2], DU Yan (杜岩)[1], XIE Qiang (谢强)[1, 3], ZHUANG Wei (庄伟)[1], WANG Dongxiao (王东晓)[1, **]

[1] *State Key Laboratory of Tropical Oceanography, South China Sea Institute of Oceanology, Chinese Academy of Sciences, Guangzhou 510301, China*

[2] *Guy Carpenter Asia-Pacific Climate Impact Centre, School of Energy and Environment, City University of Hong Kong, Hongkong, China*

[3] *Sanya Institute of Deep-sea Science and Engineering, Chinese Academy of Sciences, Sanya 572000, China*

Received Nov. 28, 2011; accepted in principle Jan. 6, 2012; accepted for publication Jun. 8, 2012

Abstract Using hydrographic data sampled during four successive late summer-early autumn cruises in 2004–2007, vertical stratification along transects in the lee of Taiwan Island was analyzed to investigate upper ocean responses to orographically induced dipole wind stress curl (WSC). Results indicate that mixed-layer depth (MLD) and its relationship with thermocline depth varied under different local wind forcings. Average MLD along the transects from the 2004 to 2007 cruises were 18.5, 30.7, 39.2 and 24.5 m, respectively. The MLD along the transects deepened remarkably and resulted in thermocline ventilation in 2005 and 2006, whereas ventilation did not occur in 2004 and 2007. Estimates indicate that frictional wind speed was the major factor in MLD variations. To a large degree, the combined effects of frictional wind speed and Ekman pumping are responsible for the spatial pattern of MLD during the cruises.

Keyword: Taiwan Island; dipole wind stress curl; mixed layer depth; thermocline

1 INTRODUCTION

Taiwan Island is bounded by Luzon Strait to the south, the East China Sea to the north, Pacific Ocean to the east, and Taiwan Strait to the west. To the southwest of the island is the South China Sea (SCS), the largest marginal sea in the Pacific Ocean. The topography of Taiwan Island features a north-south mountain range (Fig.1) with the highest peak at 3 950 m. To the west of Taiwan Strait, mainland China is characterized by plains, highlands and ridges, for which the average elevation is about 500 m. These orographic features yield a unique wind field during the northeasterly monsoon. With mountains on both sides of the strait, a strong wind jet develops over it and extends downstream, caused by canalization (Zhang, 1997). A weaker jet emerges at the southern tip of Taiwan Island. In the lee of the island, a wake of weak winds forms, owing to the blockage of high mountains. The weak winds in the wake and strong winds at its flanks result in a dipole wind stress curl (WSC) pattern, with positive curl to the north and negative curl to the south (Liu et al., 1999; Wang et al., 2008).

Previous studies have noted significant ocean responses to orographically induced wind/island wakes in various parts of the world ocean, including near the Hawaiian Islands (Xie et al., 2001), Irminger Sea (Pickart et al., 2003; Martin et al., 2007), and Arabian Sea (Luis and Kawamura, 2004). In the SCS, the importance of orographic effects on regional circulation and climate has also been revealed from

* Supported by the Knowledge Innovation Program of Chinese Academy of Sciences (No. KZCX2-YW-Q11-02), the National Basic Research Program of China (973 Program) (No. 2011CB403503), and the National Natural Science Foundation of China (Nos. 40876009, 41176028)
** Corresponding author: dxwang@scsio.ac.cn

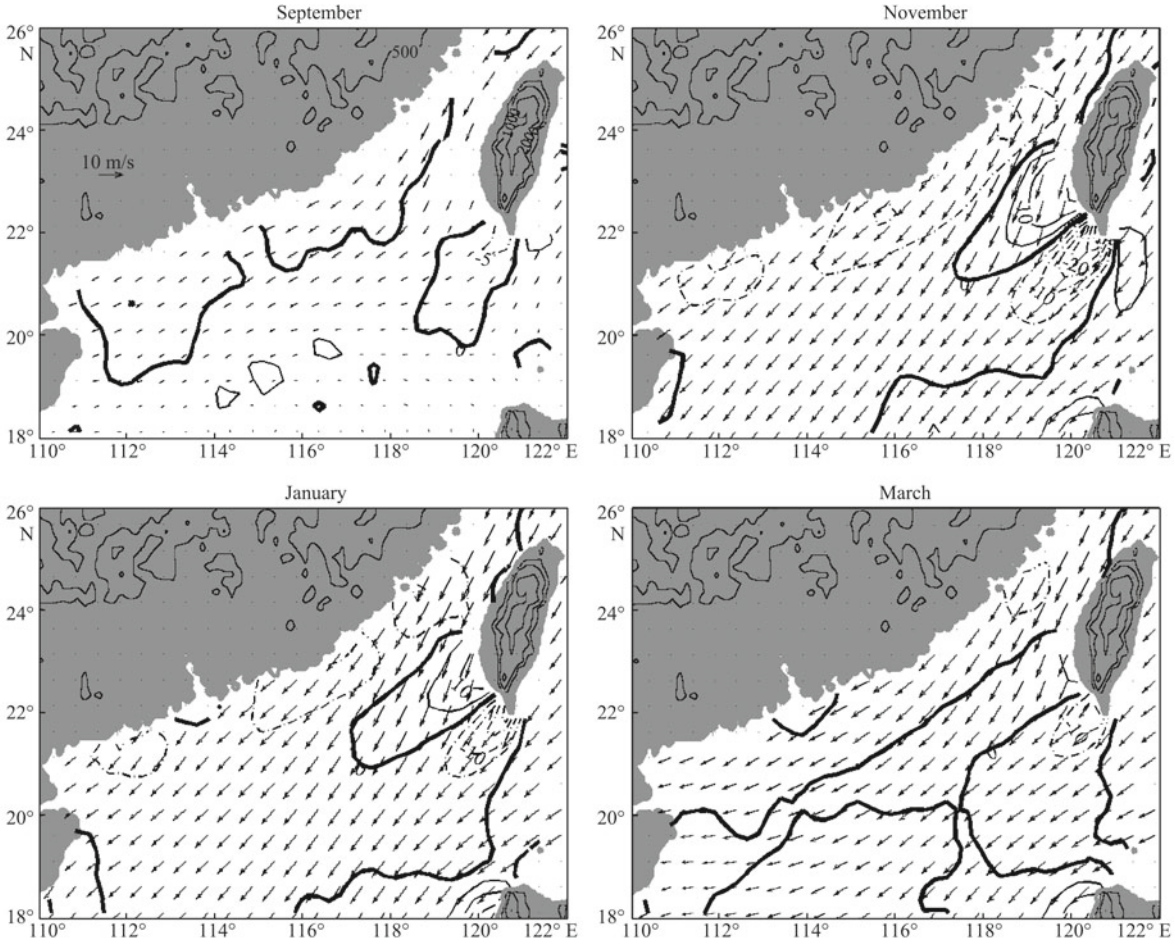

Fig.1 Climatological monthly QuikSCAT wind speed (vector) and wind stress curl (contours at 5×10^{-7} N/m^3 intervals) in September, November, January and March, averaged over 1999–2008

high-resolution satellite observations (Xie et al., 2003; Xu et al., 2008). In the western SCS, southwesterlies are blocked by the Annamese Cordillera during boreal summer, and accelerate to form a wind jet on the south edge of this mountain range (Xie et al., 2003). The resultant WSC dipole drives a double gyre in the ocean, which has been well-captured by in-situ observations (Fang et al., 2002) and reproduced by model simulations (Xu et al., 2008). In the eastern SCS, blockages of the northeast monsoon by mountains on the islands of Taiwan Island and Luzon also induce strong WSC dipoles that drive alternating clusters of cyclonic and anticyclonic eddies (Wang et al., 2008). In-situ current measurements near the southern tip of Taiwan Island revealed significant intraseasonal variations of ocean current associated with local wind curls (Wu and Chiang, 2007). However, previous works have mostly focused on responses of SCS ocean circulation and eddies to orographic winds. Impacts of these winds on thermodynamic processes in the SCS, especially oceanic stratification, are rarely investigated.

Mixed layer depth (MLD) is a useful indicator of hydrographic response to the atmosphere. In the SCS, MLD is strongly modulated by the East Asian Monsoon (Qu, 2001). In recent decades, the SCS MLD has been studied mostly with a climatological description based on relatively coarse-resolution historical datasets (Qu, 2001; Du, 2002; Qu et al., 2007). Qu et al. (2007) showed that local Ekman pumping appears to be an important process responsible for semiannual variation, which is the strongest variation in the southern SCS. However, specific effects of orographic wind on MLD variations in the northeast SCS are still not well understood.

The motivation for this study is therefore to make a high-resolution depiction of upper ocean response to the Taiwan Island dipole wind pattern of late summer-early autumn. First, MLD variations and their

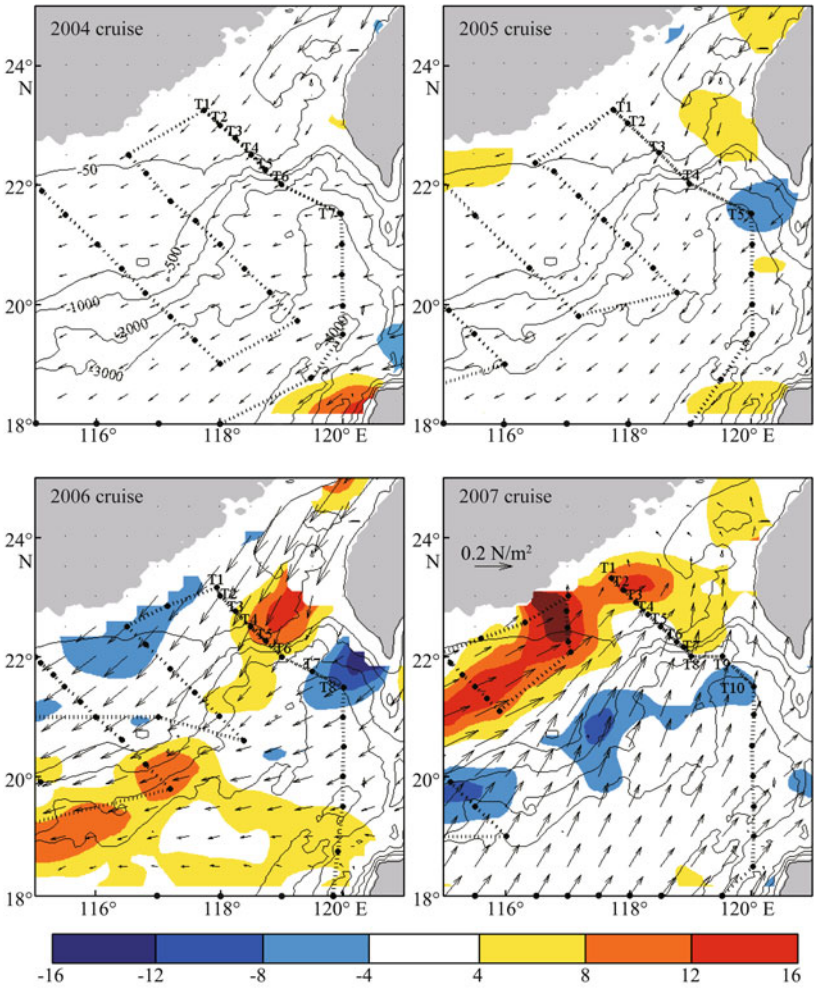

Fig.2 Map of ship tracks (dashed lines) and CTD stations (bold dots) during 2004–2007 cruises in northeastern SCS

Stations along transect T are marked. Bottom topography in this area is shown by thin solid lines (m). Vectors and shading represent mean QuikSCAT wind velocity (m/s) and WSC ($\times 10^{-7}$ N/m^3) during four cruises.

relationship with the thermocline are described with the synergy of satellite and hydrographic data. Then, we use a one-dimensional mixed layer model to investigate related dynamic and thermodynamic mechanisms for MLD variations and associated upper ocean thermal structure.

2 DATA AND METHOD

The sea surface wind product used in this study was measured by the QuikSCAT satellite scatterometer. It was launched in June 1999 and measures surface wind velocity with high resolution and accuracy (Liu, 2002). Sea surface temperature (SST) data were obtained from the Tropical Rainfall Measuring Mission (TRMM) satellite Microwave Imager (TMI) product, available since December 1997. Both original swath datasets were mapped to a 0.25°×0.25° grid by Remote Sensing Systems (RSS).

The in-situ observational data used were sampled during four cruises in the northern SCS carried out by the South China Sea Institute of Oceanology (SCSIO), Chinese Academy of Sciences (CAS). These four multidisciplinary oceanographic surveys were conducted by the R/V *Shiyan 3* in late summer-early autumn 2004–2007, with observational periods September 16–October 4, September 5–23, September 7–29, and August 10–30. These field experiments involved ship-mounted Acoustic Doppler Current Profiler (ADCP) and Conductivity-Temperature-Depth (CTD) sensors on the R/V *Shiyan 3* to measure flow speed, temperature, and salinity profiles. The distribution of CTD stations and ship tracks is shown in Fig.2. We mainly focused on transect T, which is to

the lee of Taiwan Island, where direct impacts of dipole WSC could be recorded. Vertical profiles of temperature and salinity sampled during four different cruises were used to calculate MLD. It is defined using a variable ρ criterion for a 0.5°C temperature change based on temperature dependence of the thermal expansion of surface seawater (Monterey and Levitus, 1997).

A classical Kraus-Turner mixed layer model is used to investigate the influences of dynamic forcing, thermodynamic forcing, and freshwater flux (the sum of the latter two is called buoyancy flux) on MLD (Kraus and Turner, 1967):

$$\int_{-h_m}^{0} \frac{\mathrm{dTKE}}{\mathrm{d}t}\mathrm{d}z = \mathrm{m}_3 u_*^3 - \frac{1}{2}\frac{\mathrm{g}\alpha}{\rho_s C_p} Q_{net} h_m , \quad (1)$$

where TKE is turbulence kinetic energy that controls MLD variability. The first term on the right side is the shear production of TKE generated by surface wind stress τ, where $u_*^3 = \tau/\rho_a$ is ocean friction velocity and ρ_a air density. The second term is the enhancement or damping of TKE by surface buoyancy forcing (Kara et al., 2000). Q_{net} is derived from surface radiative fluxes from National Centers for Environmental Prediction/National Center for Atmospheric Research (NCEP/NCAR) reanalysis, and from surface heat fluxes computed with the TOGA/COARE 3.0 bulk-flux algorithm (Fairall et al., 1996). MLD (h_m) and seawater density (ρ_s) are derived from in-situ temperature and salinity data. Other parameters in Eq.1 are defined as follows: m_3=7.5, g=9.81 m/s^2, α=2.5×10^{-4}/°C, ρ_a=1.21 kg/m^3, and C_p=3 988 J/(kg·°C).

3 RESULT

3.1 Seasonal evolution of dipole WSC

Figure 1 shows the evolution of climatological wind speed and WSC in the northern SCS from September to March, based on QuickSCAT observations. It is clear that the dipole WSC to the lee of Taiwan Island forms in September, strengthens in October, reaches its peak in November–December, maintains high intensities in January–February, and begins to weaken from March onward. Since September is a transition month when the monsoon veers from southwesterly to northeasterly, the dipole WSC appears intermittently during this period. Its strength is closely related to onset time of the northeast monsoon. That is, when the winter monsoon bursts earlier (later), the dipole WSC will be stronger (weaker) in September.

3.2 Hydrographic response to dipole wind patterns

Mean wind fields during the 2004–2007 cruises in the northeastern SCS exhibited significant differences (Fig.2). Sea surface wind stress during the 2004 cruise showed a weak northeasterly flow, and there was no clear WSC dipole to the lee of Taiwan Island. During the 2005 cruise, northeasterly flow occurred south of Taiwan Island. However, the WSC dipole was weak. When strong northeasterly winds appeared on the 2006 cruise, the orographic effect resulted in a conspicuous WSC dipole. During the 2007 cruise, southwesterlies occupied the northeast SCS and there was no orographic wind jet to the lee of the island. Therefore, dipole wind patterns emerged during the 2005 and 2006 cruises, but were absent during the 2004 and 2007 cruises.

Distributions of temperature and salinity along transect T had different characteristics on the four cruises (Fig.3). Around 118.5°E (T4 on the 2004 cruise), protuberant isotherms and isohalines implied the existence of subsurface upwelling in September 2004. The 25°C isotherm reached about 25 m. In the eastern part of transect T, warm water (>29°C) was confined to the upper 10 m. The surface temperature difference along the entire transect was small (~0.5°C), while surface salinity showed two low value centers near the coast (T1 and T5). During the 2005 cruise, the upwelling around 118.5°E (T3 on the 2005 cruise) was much weaker than that in 2004. The 25°C isotherm only reached 40 m depth. The 29°C contour largely deepened east of 119°E. The surface temperature difference reached 2°C. Upper salinity decreased shoreward, with a front between T2 and T3. Thermal features during the 2006 cruise were similar to those of 2005, with larger strength under a stronger northeast monsoon and dipole WSC. The 25°C isotherm was restricted beneath 60 m. During the 2007 cruise, temperature and salinity distributions along transect T were generally similar to those in 2004. The subsurface upwelling around 118.5°E intensified again. East of 119°E, vertical mixing of upper warm and fresh water was relatively weak.

The MLD distributions also showed a clear difference between the four cruises, except for shoaling to the west of 118.5°E. On the 2004 cruise, MLD along transect T was never deeper than 30 m, with an average of 18.5 m. The shallowest MLD of 11 m was around 118.5°E, resulting from local subsurface upwelling. On the 2005 cruise, the transect mean MLD was 30.7 m, much deeper than that in 2004. The region around 118.5°E also had the

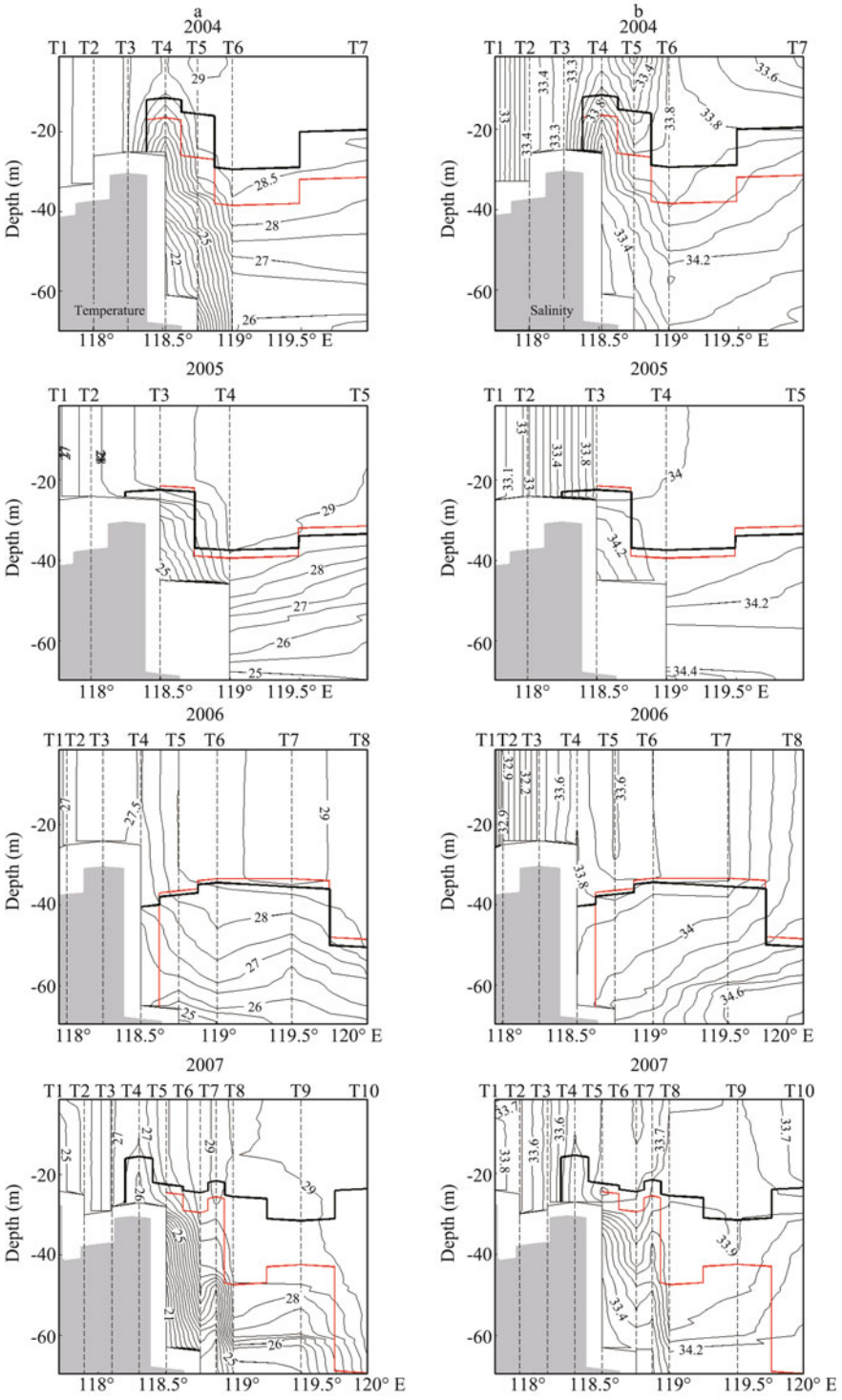

Fig.3 Temperature (a) and salinity (b) along transect T from the surface to 70 m, during 2004, 2005, 2006, and 2007 cruises

Contours show temperature at 0.5°C intervals in (a), and salinity at 0.1 intervals in (b). Gray shadings represent terrain areas. Thick curves denote MLD, and red curves the upper boundary of thermocline.

shallowest MLD of 22 m, twice that in 2004. The deepest MLD, about 40 m, occurred in the region around 119°E (T4 on the 2005 cruise). With a strong dipole wind pattern during 2006, MLD was the deepest (39.2 m) of all cruises. There was no protuberant MLD around 118.5°E during this period. The deepest MLD reached 50 m around 120°E (station T8). During the 2007 cruise, the MLD along

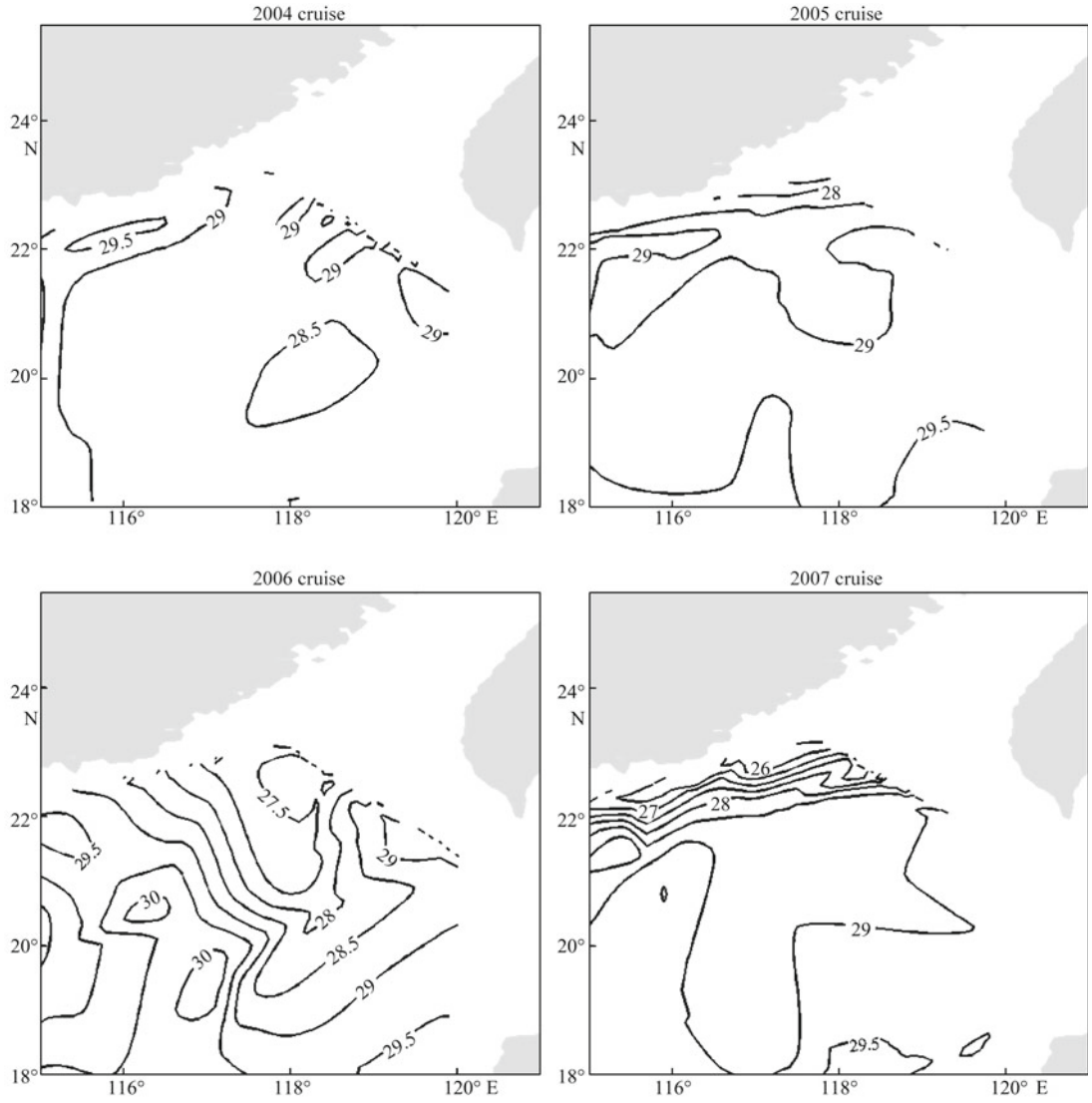

Fig.4 Near-surface (5-m depth) temperature (°C) based on CTD observations during 2004, 2005, 2006, and 2007 cruises

Contour interval is 0.5°C.

transect T had a similar structure as that on the 2004 cruise. The average MLD was 24.5 m, and the shallowest MLD (15 m) was at 118.3°E.

The oceanic thermocline is defined by a criterion of vertical temperature gradient. In this study, the criteria -0.05°C/m in deep ocean (>500 m) and -0.2°C/m in shallow seas (Liu et al., 2001) were adopted for definition of the thermocline layer. Along transect T, the deep ocean segment is east of 118.75°E. The mean upper boundary of the thermocline among these four cruises changed less than the MLD. However, its distribution along the transect in 2006 contrasted with that in 2004. Relationships between MLD and thermocline were much different among the four cruises. During the 2004 cruise, MLD detached from the thermocline markedly, with a maximum of 12 m. On the contrary, they were completed connected in the deep ocean in 2006. In particular, the MLD interposed with a strong thermocline of temperature gradient -0.2°C, suggesting thermocline ventilation. This ventilation was also observed on the 2005 cruise. The 2007 cruise was similar to that of 2004, when there was no outcropping of thermocline water. Overall, during the four cruises, thermocline ventilations occurred simultaneously with the Taiwan Island dipole wind.

Hydrographic response to various dipole wind patterns varied significantly, as revealed by near-surface (5 m) temperature obtained from the 2004–2007 cruises (Fig.4). The temperature nearly surpassed 29°C along the coast, and there was no front in the northeast SCS in 2004. When cold water (~27.5°C)

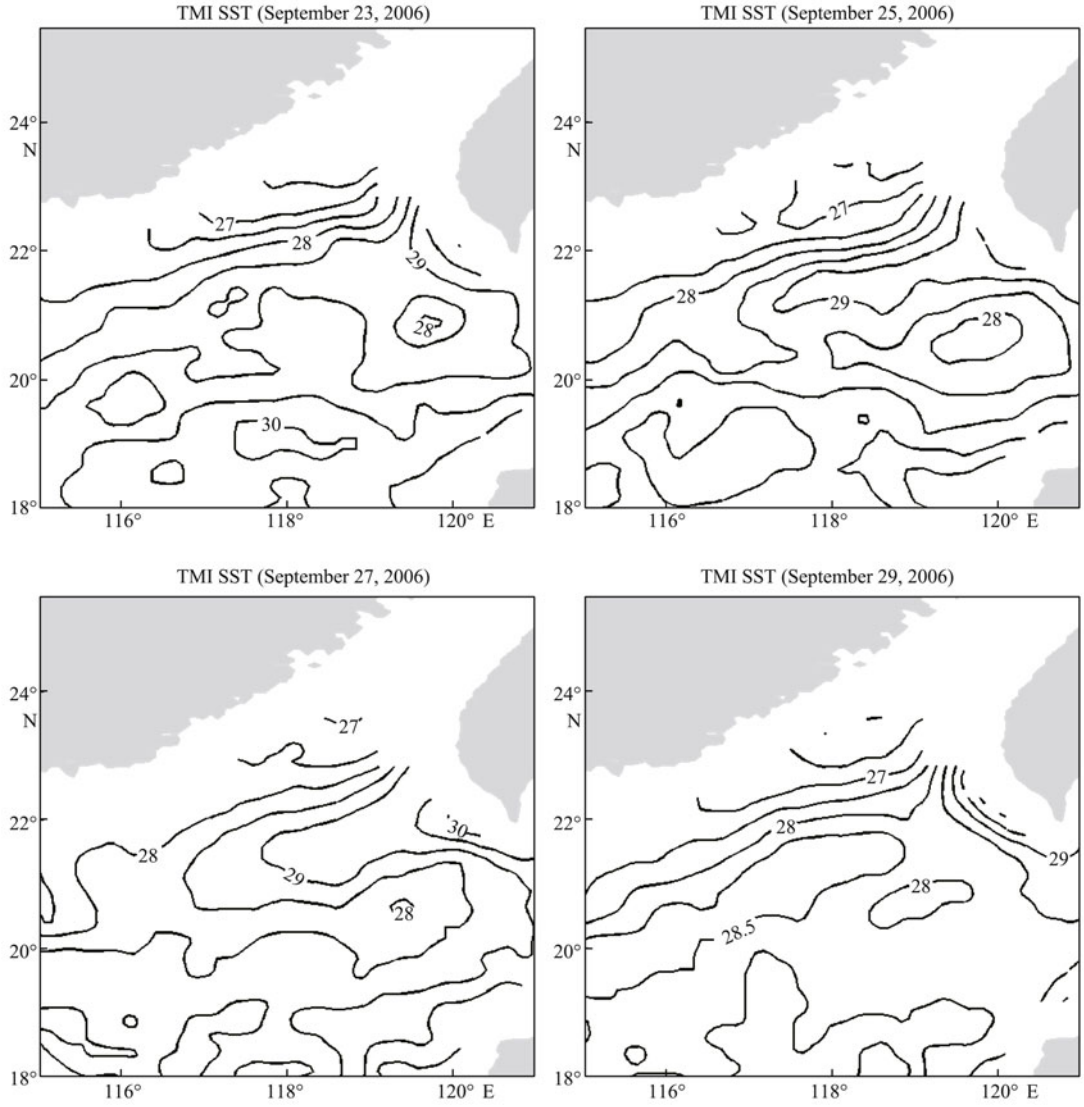

Fig.5 Daily TMI SST (°C) during 2006 cruise

Contour interval is 0.5°C

entered the northeast SCS coastal region from Taiwan Strait in 2005, it encountered warm water (>29°C) around the southern tip of Taiwan Island and formed a zonal front, which was detected in satellite SST observations (Wang et al., 2001a). During the 2006 cruise, a warm tongue (>29°C) appeared in the area of negative WSC. Combining with daily TMI SST images, the analysis showed that the warm tongue strengthened from September 24–28 and decayed after September 29 (Fig.5). Under the remarkable positive WSC, a cold tongue also emerged to the northwest of the warm one. On the 2007 cruise, nearshore cold water probably resulted from coastal upwelling driven by prevailing southwesterlies. There was a strong thermal front between the coastal cold water and homogeneous warm water in the open ocean.

3.3 Factors influencing MLD

Several air-sea interaction factors were considered for their roles in dynamic and thermodynamic mechanisms of MLD variability. Wind stress and surface buoyancy flux are related to MLD directly, while Ekman horizontal current and Ekman pumping have indirect impacts. First, results of the Kraus-Turner mixed layer model show that the effect of wind stress was largely responsible for MLD changes (Fig.6a). Averages of the cube of friction velocity (denoted as U^*) were 4.0, 8.3 and 30.7 ($\times 10^{-3}$ m^3/s^3) on the 2004, 2005 and 2006 cruises, respectively, in accord with the deepening trend of transect-mean MLD. On the 2007 cruise, U^* was 28.4×10^{-3} m^3/s^3, but MLD only reached 24.5 m. This suggests that there

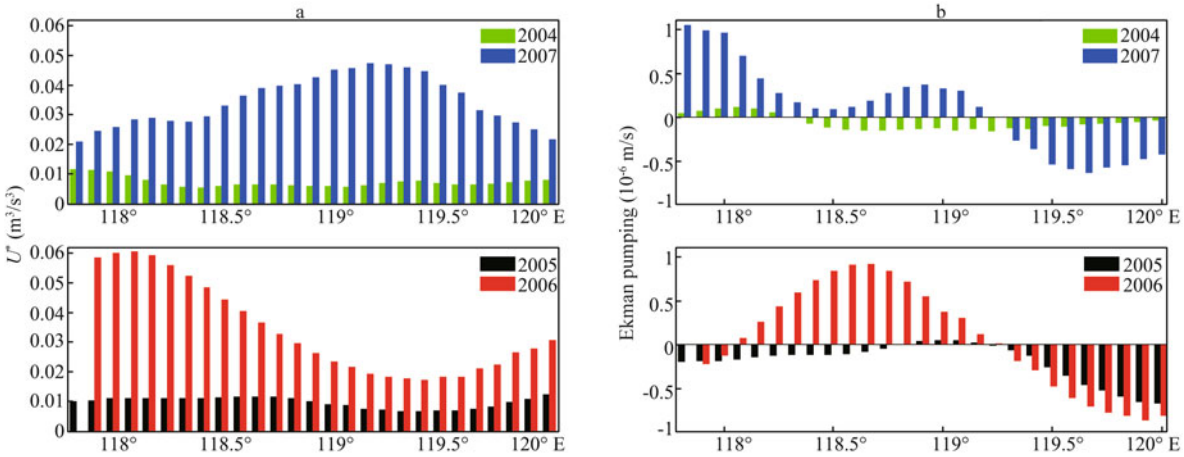

Fig.6 Factors influencing MLD along transect T during 2004, 2005, 2006, and 2007 cruises: a. Cube of ocean friction velocity, i.e., U^* (m^3/s^3); b. Ekman pumping (10^{-6} m/s)

were other factors modulating the MLD distribution. However, surface buoyancy flux estimated from the same model was much smaller (~10^{-8} m^3/s^3), and could be ignored by comparison with the cube of friction velocity (not shown).

The direction of surface Ekman flow is determined by wind direction, whereas the structure of WSC dominates Ekman pumping, i.e., convergence and divergence in the upper ocean. These two processes can also influence the MLD and thermocline in the northern SCS (Du, 2002). In addition to strong friction velocity, downwelling caused by negative Ekman pumping in the eastern part of the transect was responsible for local deepening of MLD and thermocline depth in 2005 and 2006 (especially at point T8 of the 2006 cruise). MLD east of T8 was shallower, which might be attributed to local positive Ekman pumping. Additionally, thermocline distribution in 2007 appeared consistent with Ekman pumping effects (Fig.6b). Similar to the factors determining semiannual variation of MLD in the southern SCS (Qu et al., 2007), local Ekman pumping is important to MLD variations in the northeast SCS. The former is associated with orographic wind caused by the Annamese Cordillera during the summer monsoon (Xie et al., 2003). The latter is dominated by the effect of Taiwan Island dipole wind patterns, which are components of orographic wind jets in the eastern SCS during northeasterlies (Wang et al., 2008). On the other hand, northwestward Ekman horizontal transport possibly played an important role in the local MLD deepening during 2005 and 2006, especially from 119°–120°E. To the west of 118.5°E in those years, the Ekman horizontal transport was toward the southwest, because its direction should match that of local wind in shallow water of depth less than half the Ekman layer (not shown).

4 DISCUSSION

Based on a climatological hydrographic dataset, Wang et al. (2001b) noted seasonal thermocline ventilation in the northern SCS. It occurs during the northeast monsoon, owing to pronounced surface cooling. Consequently, the subduction water mass moves southwestward along isolines of potential vorticity. Here, we further demonstrated that thermocline ventilation on the synoptic timescale can also occur to the lee of Taiwan Island during early autumn. This is not attributed to surface cooling, but is mainly induced by the strong orographic wind jet to the southwest of Taiwan Island.

Southeast of Taiwan Island, circulation and water mass are also affected by the Kuroshio intrusion (Shaw, 1991; Qu et al., 2001). In addition, there is great mesoscale variability in this region (Yuan et al., 2007; Zhuang et al., 2010). Possible mechanisms for local eddy generation include: Kuroshio-topography interactions (Jia et al., 2005), Kuroshio-eddy interactions in the Western Pacific (Yuan et al., 2006), and WSC forcing, which may reflect the indirect effect of orographic wind on stratification (Wu and Chiang, 2007). Considering that the dipole WSC (Fig.2) and resulting Ekman pumping were relatively weak in 2004, the evidence of strong upwelling and downwelling probably resulted from the impact of Kuroshio intrusions. This deserves further investigation, with increased observational and modeling efforts. This study only focused on the

direct impact of wind forcing on stratification structures. The potential influence of other physical processes should be evaluated in future works.

5 CONCLUSION

During the northeast monsoon, as winds impinge on the mountain ranges of Taiwan Island, orographic blockage accelerates the wind at its southern tip, forming the dipole WSC. This paper reports different upper ocean hydrographic structures under various conditions of Taiwan Island dipole wind, based on observational data during four late summer-early autumn cruises during 2004–2007. Transect-mean MLDs were 18.5, 30.7, 39.2 and 24.5 m, respectively. MLD deepening during the 2005 and 2006 cruises resulted in thermocline ventilation.

Further analysis based on a mixed layer model suggested that wind stress has significant impacts on MLD changes. During the 2004–2006 cruises, the deepening trend of the MLD was consistent with strengthening U^*. On the 2007 cruise, wind stress curl appeared to have a more significant role in the variation of MLD and the thermocline. Corresponding to the spatial pattern of Ekman pumping, thermocline depth shoaled westward along transect T. Thermodynamic forcing has a minor role in establishing the ventilated thermocline, compared with dynamic forcing. Further studies will attempt to quantify the relative importance of direct orographic wind forcing and other processes (e.g., Kuroshio intrusion, eddy activities), through use of a high-resolution general circulation model.

References

Du Y. 2002. Seasonal dynamics of the mixed layer and thermocline in the South China Sea, Ph.D. dissertation, Ocean Univ. of China, Qingdao. 240p.

Fairall C W, Bradley E, Rogers D P, Edison P J B, Young G S. 1996. Bulk parameterization of the air-sea fluxes for tropical ocean-global atmosphere coupled-ocean response experiment. *Geophys. Res. Lett.*, **101**: 3 747-3 764.

Fang W, Fang G, Shi P, Huang Q, Xie Q. 2002. Seasonal structures of upper layer circulation in the southern South China Sea from in situ observations. *J. Geophys. Res.*, **107**: 3 202, http://dx.doi.org/10.1029/2002JC001343.

Jia Y, Liu Q, Liu W. 2005. Primary study of the mechanism of eddy shedding from the Kuroshio Bend in Luzon Strait. *J. Oceanogr.*, **61**: 1 017-1 027.

Kara A B, Rochford P A, Hurlburt H E. 2000. Mixed layer depth variability and barrier layer formation over the North Pacific Ocean. *J. Geophys. Res.*, **105**(C7): 16 783-16 802.

Kraus E B, Turner J S. 1967. A one-dimensional model of the seasonal thermocline. Part II: The general theory and its consequences. *Tellus*, **19**: 98-105.

Liu Q, Jia Y, Liu P, Wang Q. 2001. Seasonal and interseasonal thermocline variability in the central South China Sea. *Geophys. Res. Lett.*, **28**(23): 2 267-4 470.

Liu W T. 2002. Progress in scatterometer application. *J. Oceanogr.*, **58**: 121-136, http://dx.doi.org/10.1023/A:1015832919110

Liu W T, Xie X. 1999. Space-based observations of the seasonal changes of South Asian monsoons and oceanic response. *Geophys. Res. Lett.*, **26**: 1 473-1 476.

Luis A J, Kawamura H. 2004. Air-sea interaction, coastal circulation and primary production in the eastern Arabian Sea: a review. *J. Oceanogr.*, **60**: 205-218.

Martin R, Moore G W K. 2007. Air-sea interaction associated with a Greenland reverse tip jet. *Geophys. Res. Lett.*, **34**, L24802, http://dx.doi.org/10.1029/2007GL031093.

Monterey G, Levitus S. 1997. Seasonal variability of mixed layer depth for the World Ocean. NOAA Atlas NESDIS 14, U.S. Gov. Printing Office, Wash. DC. 100p.

Pickart R S, Spall M A, Ribergaard M H, Moore G W K, Milliff R F. 2003. Deep convection in the Irminger Sea forced by the Greenland tip jet. *Nature*, **424**(6 945): 152-156.

Qu T. 2001. The role of ocean dynamics in determining the mean seasonal cycle of the South China Sea surface temperature. *J. Geophys. Res.*, **106**: 6 943-6 955.

Qu T, Du Y, Gan J, Wang D. 2007. Mean seasonal cycle of isothermal depth in the South China Sea. *J. Geophys. Res.*, **112**: C02020, http://dx.doi.org/10.1029/2006JC003583.

Shaw P-T. 1991. Seasonal variation of the intrusion of the Philippine Sea water into the South China Sea. *J. Geophys. Res.*, **96**: 821-827.

Wang B, Wu R, Fu X. 2000. Pacific-East Asian teleconnection: how does ENSO affect East Asian climate? *J. Clim.*, **13**: 1 517-1 536.

Wang D, Liu Y, Qi Y, Shi P. 2001a. Seasonal variability of thermal fronts in the northern South China Sea from satellite data. *Geophys. Res. Lett.*, **28**(20): 3 963-3 966.

Wang D, Du Y, Shi P. 2001b. Evidence for thermocline ventilation in the South China in winter, *Chin. Sci. Bull.*, **46**(9): 774-778.

Wang G, Chen D, Su J. 2008. Winter eddy genesis in the eastern South China Sea due to orographic wind jets. *J. Phys. Oceanogr.*, **38**: 726-732.

Wu C-R, Chiang T L. 2007. Mesoscale eddies in the northern South China Sea. *Deep Sea Res., Part II*, **54**: 1 575-1 588.

Xie S-P, Liu W T, Liu Q, Nonaka M. 2001. Far-reaching effects of the Hawaiian Island on the Pacific Ocean-Atmosphere. *Science*, **292**: 2 057-2 060.

Xie S-P, Xie Q, Wang D, Liu W T. 2003. Summer upwelling in the South China Sea and its role in regional climate variations. *J. Geophys. Res.*, **108**: 3 261, http://dx.doi.org/10.1029/2003JC001867.

Xu H, Xie S-P, Wang Y, Zhuang W, Wang D. 2008. Orographic effects on South China Sea summer climate. *Meteorol. Atmos. Phys.*, **100**: 275-289.

Yuan D, Han W, Hu D. 2006. Surface Kuroshio path in the Luzon Strait area derived from satellite remote sensing data. *J. Geophys. Res.*, **111**: C11007, http://dx.doi.org/10.1029/2005JC003412.

Yuan D, Han W, Hu D. 2007. Anti-cyclonic eddies northwest of Luzon in summer-fall by satellite altimeters. *Geophys. Res. Lett.*, **34**: L13610, http://dx.doi.org/10.1029/2007GL029401.

Zhang Y. 1997. East Asian winter monsoons: results from eight AMIP models. *Clim. Dyn.*, **13**: 11 797-11 820.

Zhuang W, Xie S P, Wang D, Taguchi B, Aiki H, Sasaki H. 2010. Intraseasonal variability in sea surface height over the South China Sea. *J. Geophys. Res.*, **115**: C04010, http://dx.doi.org/10.1029/2009JC005647.